Radial Structure of Alfvén Eigenmodes in the DIII-D Tokamak through Electron-Cyclotron-Emission Measurements

M. A. Van Zeeland,[1,*] G. J. Kramer,[2] M. E. Austin,[3] R. L. Boivin,[4] W. W. Heidbrink,[5] M. A. Makowski,[6] G. R. McKee,[7] R. Nazikian,[2] W. M. Solomon,[2] and G. Wang[8]

[1]*Oak Ridge Institute for Science Education, P.O. Box 117, Oak Ridge, Tennessee 37831-0117, USA*
[2]*Princeton Plasma Physics Laboratory, P.O. Box 451, Princeton, New Jersey 08543, USA*
[3]*Institute for Fusion Studies, University of Texas, Austin, Texas, USA*
[4]*General Atomics, P.O. Box 85608, San Diego, California 92186-5608, USA*
[5]*University of California, Irvine, California, USA*
[6]*Lawrence Livermore National Laboratory, Livermore, California 94550, USA*
[7]*University of Wisconsin, Madison, Wisconsin 53706, USA*
[8]*University of California, Los Angeles, California 90095, USA*

(Received 16 May 2006; published 25 September 2006)

The spatial structure of toroidal Alfvén eigenmodes and reversed shear Alfvén eigenmodes in DIII-D is obtained from electron-cyclotron-emission measurements. Peak measured temperature perturbations are of similar magnitude for both toroidal Alfvén eigenmodes and reversed shear Alfvén eigenmodes and found to be $\delta T_e/T_e \approx 0.5\%$. Simultaneous measurements of density fluctuations using beam-emission spectroscopy indicate $\delta n_e/n_e \approx 0.25\%$. Predictions of the measured temperature and density perturbation profiles as well as $\delta T_e/\delta n_e$ from the ideal magnetohydrodynamic code NOVA are in close agreement with experiment.

DOI: 10.1103/PhysRevLett.97.135001 PACS numbers: 52.55.Fa, 52.35.Bj, 52.35.Kt, 52.55.Pi

Future burning plasma experiments such as ITER may be subject to the excitation of Alfvén instabilities by 3.5 MeV fusion-born alpha particles, injected neutral beam ions [1], and the thermal plasma ions themselves [2]. These instabilities can cause enhanced fast-ion transport leading to possible serious damage of first wall components [1] as well as potentially advantageous current profile modifications [3]. In order to have confidence in our ability to predict Alfvénic activity and its nonlinear consequences in future devices, as well as to obtain valuable information about the plasma equilibrium via magnetohydrodynamic (MHD) spectroscopy [4], a detailed understanding of the internal structure of Alfvén eigenmodes (AEs) is essential. Recently, much progress has been made related to AE detection in tokamak plasmas; in particular, several density fluctuation diagnostic systems on various tokamaks have reported measurements of both reversed shear Alfvén eigenmodes (RSAEs) and toroidal Alfvén eigenmodes (TAEs) [2,5–7]. However, with the exception of multichannel reflectometry [8], no localized measurements of the detailed radial structure of these modes has been presented.

This Letter is concerned with the use of the DIII-D electron-cyclotron-emission (ECE) radiometer to measure electron temperature fluctuations which result from the magnetic field line displacement (ξ) and adiabatic compression of shear Alfvén modes. The AE temperature perturbation is given by:

$$\frac{\delta T_e}{T_e} = -(\gamma - 1)\nabla \cdot \xi - \xi \cdot \frac{\nabla T_e}{T_e}, \qquad (1)$$

where T_e is the electron temperature and $\gamma = 5/3$ is the ratio of specific heats [9,10]. Previous studies utilizing the perturbed ECE to probe AEs have been successful [11,12] and through correlation techniques with magnetic probes have obtained information on the mode location [13]. The newly upgraded ECE heterodyne radiometer on DIII-D obtains detailed structural information on AEs using a total of 40 radially spaced channels across the plasma midplane [14].

Figure 1 displays power spectra from two ECE channels located on the low-field side of the magnetic axis at different minor radii as well as a Mirnov loop located on the outboard midplane. These data are taken during the early phase of neutral beam injection. Throughout the time window shown, 4.6 MW, 78 keV, sub-Alfvénic neutral deuterium beams are injected during the current rise phase of the discharge and the central magnetic shear is reversed, i.e., $S \cong (r/q)(dq/dr) < 0$, where q is the safety factor. The inner ($\rho = 0.45$) and outer ($\rho = 0.64$) ECE spectra exhibit extremely different behavior and the outer Mirnov spectrum shows characteristics of both signals. There are at least two types of Alfvén eigenmodes present in the discharge. The series of relatively constant frequency modes beginning around 80 kHz in Figs. 1(a) and 1(c) has been identified by comparison to ideal MHD calculations as TAEs of various toroidal mode numbers (n). The approximate overplotted TAE frequency near $q_{\min}$ is calculated according to $f_{\mathrm{TAE}} = V_A/4\pi q_{\min} R$, where V_A is the Alfvén speed and R is the major radius. The observed mode frequency must be corrected for toroidal rotation, which for neutral beam injection in the direction of plasma cur-

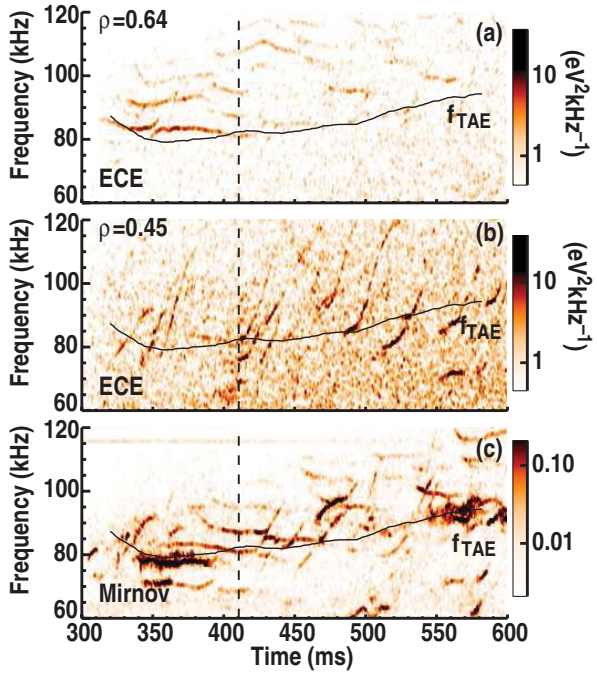

FIG. 1 (color). Discharge 122117. (a)–(b) Windowed power spectrum of ECE radiometer data at two different radial locations. Radial position (ρ = normalized square root of toroidal flux) on the outboard midplane is given for $t = 410.6$ ms (dashed vertical line). (c) Windowed power spectrum of Mirnov coil located on the outboard midplane in arbitrary units. Calculated TAE frequency (f_{TAE}) near $q_{\min}$ is overlaid (solid black line). Toroidal rotation near $q_{\min}$ increases from zero at $t = 300$ ms to $\approx$ 6–8 kHz throughout the remainder of the shown time segment. 1 kHz smoothing has been applied to all spectra.

rent shifts the mode frequencies according to $f_{\mathrm{lab}} \approx f_{\mathrm{TAE}} + n f_{\mathrm{rot}}$, where f_{rot} is the toroidal rotation frequency and f_{lab} is the mode frequency as measured in the lab frame. On the ECE spectrogram at $\rho = 0.45$, there are modes chirping up in frequency much faster than the evolution of f_{TAE}. From the temporal behavior of these modes' frequencies as well as by comparison to MHD simulations, these chirping modes have been identified as RSAEs (sometimes called Alfvén cascades). RSAEs are a class of shear Alfvén eigenmodes that exist in weak or reversed shear plasmas and are localized near minima in the magnetic safety factor ($q_{\min}$) [15]. The RSAE is composed primarily of one poloidal harmonic (m), and as $q_{\min}$ decreases, the mode transitions to a TAE with two dominant poloidal harmonics (m and $m-1$). If $q_{\min}$ continues to decrease, the TAE then follows the $q = (m-1/2)/n$ surface. In the zero pressure limit, the RSAE frequency changes as $f_{\mathrm{RSAE}} = [(m - n q_{\min}) V_A]/(2\pi q_{\min} R)$ [16,17]. Recently, much attention has been devoted to the RSAE due to its potential for diagnosing properties of the internal safety factor profile of the plasma. For example, at $t =$ 400 ms a ''grand cascade'' occurs, marked by several RSAEs of successive toroidal mode numbers appearing simultaneously, signaling the fact that $q_{\min}$ has crossed an integer value; $q_{\min} = 4$ [2,18].

Shown in Fig. 2(a) is a radial profile of ECE power spectra at $t = 410.6$ ms for the plasma in Fig. 1. Various RSAEs and TAEs are labeled along with their toroidal mode number ($n = 2$–4) obtained from Mirnov loops. Overplotted is the q profile derived from the motional Stark effect (MSE) diagnostic as well as the electron temperature. The RSAEs are clearly localized near $q_{\min}$ in Fig. 2(a), and the TAEs are seen for radii outside of $q_{\min}$ extending to the plasma edge. The localization of RSAEs near $q_{\min}$ provides a check on the MSE derived location of $q_{\min}$. Figure 2(b) shows the calculated $n = 3$ Alfvén continuum in the lab frame. The solid overlaid lines correspond to the frequencies of the $n = 3$ RSAE (blue) and both $n = 3$ TAEs (red). Each mode is seen to lie in the TAE gap as expected, and, by comparison to Fig. 2(a), the eigenmodes can be seen to only weakly intersect the continuum.

The spatial and temporal resolution of the ECE data on DIII-D affords detailed comparison to AE theory using the ideal MHD code NOVA [9,19]. As inputs, NOVA uses the measured spatial profiles of electron density, electron temperature, safety factor, ion temperature, and toroidal rotation [20] obtained from Thomson scattering, MSE, and

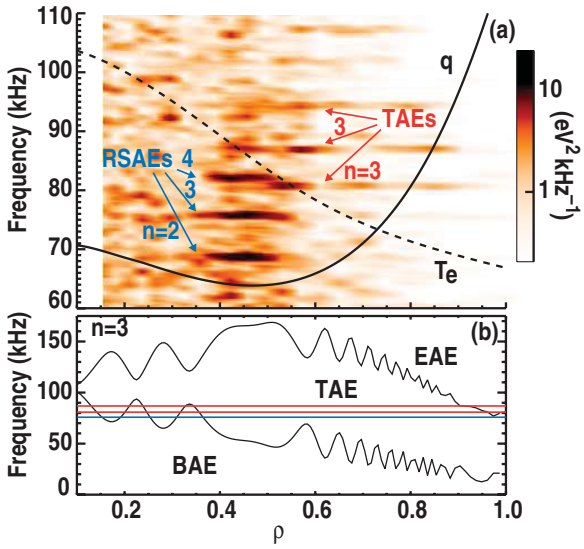

FIG. 2 (color). Discharge 122117, $t = 410.6$ ms, on axis: $T_e = 1.5$ keV, $T_i = 1.9$ keV, $B_T = 2.0$ T, $n_e = 2.17 \times 10^{13}$ cm^{-3}, $f_{\mathrm{rot}} = 9.9$ kHz. (a) Radial profile of ECE radiometer power spectra. RSAEs (blue line) and TAEs (red line) are pointed out along with toroidal mode number (n). The solid overlaid line is the safety factor profile (q) obtained through interpolation of that derived by MSE measurements at $t = 396$ and 425 ms. The dashed line is the electron temperature profile. 1 kHz smoothing has been applied. (b) $n = 3$ Alfvén continuum including toroidal rotation. The horizontal lines mark $n = 3$ RSAE (blue line) and TAE (red line) frequencies from (a).

charge exchange recombination measurements. The input equilibrium is obtained from EFIT [21] equilibrium magnetic flux reconstructions that use MSE, magnetics, and thermal pressure data. The safety factor profile used in the analysis was shifted down by $\delta q = 0.047$ from that derived by the MSE measurements—within the 10% error bars. This lowered $q_{\min}$ from 4.027 to 3.98 as to coincide with $q_{\min}$ inferred from the temporal evolution of Alfvén cascade frequencies [18]. The ideal MHD predictions for the 2D eigenmodes of δT_e corresponding to the $n = 3$ RSAE and lower frequency $n = 3$ TAE in Fig. 2 are shown in Figs. 3(a) and 3(b), respectively. Derived from these, the corresponding radial structures of the predicted temperature perturbation for the RSAE and TAE are shown along with the ECE measured eigenmode in Figs. 3(c) and 3(d), respectively. A least-squares fit was used to scale the predicted temperature perturbation eigenmode to the ECE data in Figs. 3(c) and 3(d). To convey the finite poloidal size over which the shown measurements are made and how it varies with the major radius, the microwave collection optics beam waist specified at the e^{-1} width of electric field points is shown overlaid in Figs. 3(a) and 3(b) (white lines). The beam-waist radii range from approximately 5 cm at the outer plasma edge

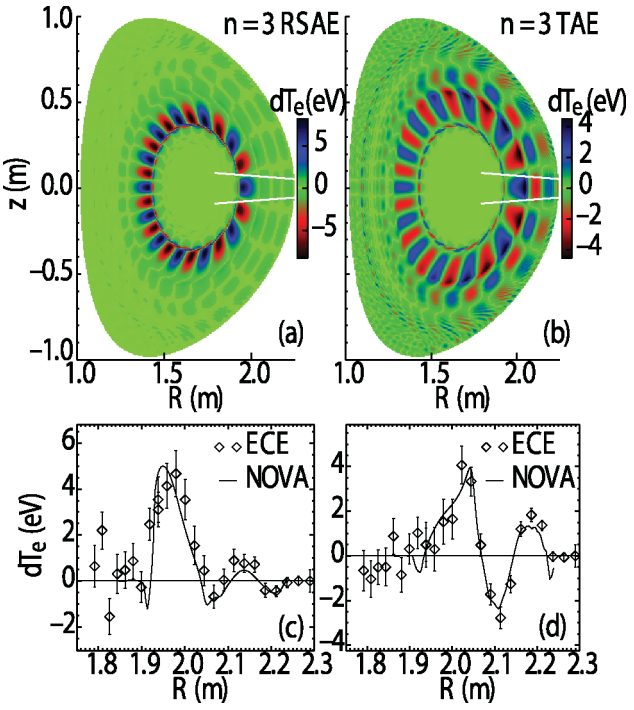

FIG. 3 (color). Discharge 122117, $t = 410.6$ ms. (a)–(b) NOVA calculated temperature perturbation for $n = 3$ RSAE and $n = 3$ TAE, respectively. The white overlaid lines show the ECE viewing optics Gaussian beam waist. (c)–(d) diamonds = ECE radiometer measured temperature perturbation; solid line = NOVA prediction for ECE radiometer temperature perturbation. Predicted eigenmode amplitude obtained by least-squares fit to the ECE data.

to 9 cm in the core. Additionally, the ECE radiometer channels themselves have a finite rf filter bandwidth ranging from 400 MHz to 1 GHz, corresponding to a radial "spot" size of 0.8–2 cm, with the exact width depending on radial position. In order to incorporate the finite ECE collection volume due to the microwave optics and rf filter widths, the MHD predictions were averaged over the corresponding spatial region assuming a Gaussian beam profile in the vertical and toroidal direction with a beam waist shown in Figs. 3(a) and 3(b) and a notchlike acceptance function in the radial direction. The simulation results shown in Fig. 3 exhibit close agreement with the measured spatial structure of the temperature perturbation for both the RSAE and TAE, including the oscillatory structure of the solutions in the radial direction. Furthermore, the predicted mode frequencies were 72.3 and 73.5 kHz for the RSAE and TAE, respectively, whereas the experimental values were 75.8 and 80.8 kHz, also in good agreement with the predictions. Such agreement with linear theory is typical for discharges in which large bandwidth low-noise ECE data are available and care is taken to obtain input profiles as accurate as possible in the modeling—specifically that of the safety factor and its precise value at $q_{\min}$. On the high-field side (HFS), the ECE antenna pattern was much larger than a poloidal wavelength resulting in a measured temperature perturbation below the noise floor. For the RSAE and TAE, the peak measured temperature perturbation on the low-field side (LFS) shown in Figs. 3(c) and 3(d) is roughly 5 and 4 eV, respectively. The ratio of the compressional to gradient terms of Eq. (1) at the peak perturbation location on the LFS (HFS) is -0.17 (0.27) for the simulated RSAE and -0.12 (0.23) for the TAE.

Independent verification of the results from another diagnostic is provided by beam-emission spectroscopy (BES) measurements of the RSAE density perturbation in a localized radial region on the plasma midplane. For this discharge, the 16 channel BES system views density fluctuations in a ≈ 4 cm $\times$ 4 cm grid centered at $(R, z) = (1.955, 0.022)$ m. The vertically spaced BES channels allow determination of the poloidal wave number. The poloidal wave number measured by BES for the $n = 3$ RSAE shown was $k_{\text{pol}} = 0.220 \pm 0.025$ cm^{-1} as compared to $k_{\text{pol}} = 0.23$ cm^{-1} predicted for the low-field side; similar agreement is obtained for the $n = 2$ and $n = 4$ RSAEs.

Also, now that the theoretical mode amplitude has been obtained by matching the predicted temperature perturbation shape to ECE data, self-consistent predictions can be made for the absolute magnitude of the density perturbation at the BES viewing locations, where the density fluctuation amplitude is given by [9]:

$$\frac{\delta n_e}{n_e} = -\nabla \cdot \xi - \xi \cdot \frac{\nabla n_e}{n_e}. \tag{2}$$

Using the mode amplitude inferred for the $n = 3$ RSAE from the ECE measurements (shown in Fig. 3) in combi-

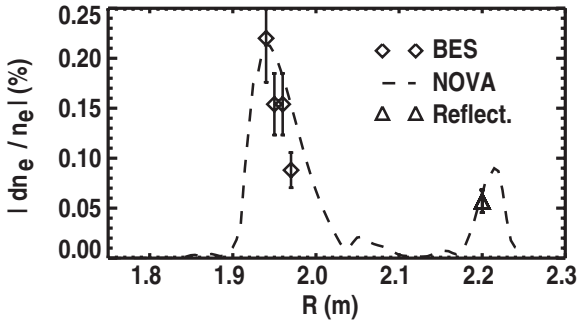

FIG. 4. The dashed line is the calculated density perturbation for the $n = 3$ RSAE in Fig. 3(c). NOVA predicted mode amplitude obtained independently via a least-squares fit to the ECE measured temperature perturbation. The triangle and diamonds are quadrature reflectometer and BES measured density fluctuation amplitudes, respectively. The electron density at the BES viewing location is approximately $n_e = 2.1 \times 10^{19}$ m^{-3}.

nation with Eq. (2), the predicted $\delta n_e/n_e$ is shown in Fig. 4 along with the measured values from BES and an additional measurement from a 65 GHz quadrature reflectometer [22]. The fact that good agreement is obtained between the measured density fluctuation and the ideal MHD predictions illustrates that the density and temperature fluctuation measurements from the different diagnostics are all consistent with the same mode amplitude. Additionally, these data effectively verify the NOVA prediction for the ratio $\delta T_e/\delta n_e$ calculated according to Eqs. (1) and (2). Consequently, the magnetic fluctuation level can be reliably obtained from the ECE measurements. The corresponding peak magnetic fluctuation amplitudes for the RSAE and TAE in Fig. 3 are $\delta B/B = (1.5 \pm 0.14) \times 10^{-4}$ and $\delta B/B = (2.5 \pm 0.18) \times 10^{-4}$, respectively.

Of particular importance in obtaining these results is the inclusion of compressive effects in the ideal MHD model used. In our calculations, we have used the canonical value of $5/3$ for γ, based on 3 degrees of freedom. A preliminary systematic γ scan and eigenmode search from $\gamma = 0.0$ to $\gamma = 2.0$ indicates little effect on the simulated TAE and a pronounced effect on the RSAE frequency, which consequently changes its coupling to the Alfvén continuum and mode structure. Specifically, we conclude that γ in the range 1.2–1.8 is most consistent with these experimental measurements.

In summary, spatially resolved ECE measurements of the electron temperature perturbation due to both RSAEs and TAEs in DIII-D have been obtained. The measured mode structures are in very close agreement with MHD calculations of the linear eigenmodes. With an amplitude inferred from ECE measurements, the same eigenmodes have also been shown to accurately predict both the magnitude and structure of the simultaneously measured density perturbation for an $n = 3$ RSAE, further validating the ideal MHD approach used in the calculations. For ITER, a similar ECE system is planned, and diagnostics capable of monitoring core Alfvénic activity beyond typical magnetic probes will be essential. These results suggest a reliable means for identifying internal AEs in "real time" by use of ECE measurements in present and future experiments, possibly in combination with ideal MHD calculations to form the basis for a matched-filter-type mode identification [23]. Additionally, this study shows that viewing geometry design in future ECE radiometers is critical in order to optimize resolution of AEs, paying particular attention to viewing beam-waist size compared to the expected poloidal wavelength of AEs.

This work was sponsored by the Department of Energy under Grants No. DE-FC02-04ER54698, No. DE-AC05-76OR00033, No. DE-AC02-76CH03073, No. DE-FG03-97ER54415, No. SC-G903402, No. W-7405-ENG-48, No. DE-FG03-96ER54373, and No. DE-FG03-01ER54615 and in part by an appointment to the U.S. Department of Energy Fusion Energy Postdoctoral Research Program administered by the Oak Ridge Institute for Science and Education.

*Electronic address: vanzeeland@fusion.gat.com

[1] K. L. Wong, Plasma Phys. Controlled Fusion **41**, R1 (1999).
[2] R. M. Nazikian *et al.*, Phys. Rev. Lett. **96**, 105006 (2006).
[3] K. L. Wong *et al.*, Phys. Rev. Lett. **93**, 085002 (2004).
[4] H. A. Holties *et al.*, Plasma Phys. Controlled Fusion **39**, 73 (1997).
[5] S. E. Sharapov *et al.*, Phys. Rev. Lett. **93**, 165001 (2004).
[6] M. A. Van Zeeland, G. J. Kramer, R. Nazikian, H. L. Berk, T. N. Carlstrom, and W. M. Solomon, Plasma Phys. Controlled Fusion **47**, L31 (2005).
[7] J. A. Snipes *et al.*, Phys. Plasmas **12**, 056102 (2005).
[8] R. M. Nazikian *et al.*, Phys. Rev. Lett. **91**, 125003 (2003).
[9] C. Z. Cheng, Phys. Rep. **211**, 1 (1992).
[10] F. F. Chen, *Introduction to Plasma Physics and Controlled Fusion* (Plenum, New York, 1984).
[11] W. W. Heidbrink, A. Fasoli, D. Borba, and A. Jaun, Phys. Plasmas **4**, 3663 (1997).
[12] V. S. Udinstev *et al.*, Plasma Phys. Controlled Fusion **48**, L33 (2006).
[13] S. E. Sharapov *et al.*, Phys. Plasmas **9**, 2027 (2002).
[14] M. E. Austin and J. Lohr, Rev. Sci. Instrum. **74**, 1457 (2003).
[15] Y. Kusama *et al.*, Nucl. Fusion **38**, 1215 (1998).
[16] H. L. Berk, D. N. Borba, B. N. Breizman, S. D. Pinches, and S. E. Sharapov, Phys. Rev. Lett. **87**, 185002 (2001).
[17] B. N. Breizman *et al.*, Phys. Plasmas **10**, 3649 (2003).
[18] M. A. Van Zeeland *et al.*, Nucl. Fusion **46**, S880 (2006).
[19] C. Z. Cheng and M. S. Chance, J. Comput. Phys. **71**, 124 (1987).
[20] G. J. Kramer *et al.*, Phys. Plasmas **13**, 056104 (2006).
[21] L. L. Lao, H. E. St. John, R. D. Stambaugh, A. G. Kellman, and W. Pfeiffer, Nucl. Fusion **25**, 1611 (1985).
[22] G. Wang *et al.*, Nucl. Fusion (to be published).
[23] D. H. Edgell, J. S. Kim, I. N. Bogatu, D. A. Humphreys, and A. D. Turnbull, Rev. Sci. Instrum. **73**, 1761 (2002).